

Cite this article as: Han Dong, Zhao Yongqing, Zeng Weidong, et al. Cellular Automata Based Microstructure Prediction in Accumulative Roll-Bonding of TA15 Sheets[J]. Rare Metal Materials and Engineering, 2021, 50(10): 3437-3445.

ARTICLE

# Cellular Automata Based Microstructure Prediction in Accumulative Roll-Bonding of TA15 Sheets

Han Dong<sup>1</sup>, Zhao Yongqing<sup>1,2</sup>, Zeng Weidong<sup>1</sup>, Li Lei<sup>2</sup>, Zhang Yongqiang<sup>2</sup>

<sup>1</sup> School of Materials Science and Engineering, Northwestern Polytechnical University, Xi'an 710072, China; <sup>2</sup> Northwest Institute for Nonferrous Metal Research, Xi'an 710016, China

**Abstract:** The influence of different cumulative rolling processes on the distribution of thermal parameters of sheet was simulated using DEFORM commercial finite element software. The dynamic globularization process of TA15 titanium alloy after thermal compression and cumulative rolling was simulated by the cellular automata. The result shows that during the accumulative roll bonding (ARB) process, the microstructure and properties of TA15 titanium alloy can be effectively improved by reducing the deformation of single pass and rolling speed as well as maintaining a certain temperature. A reasonable dynamic globularization cellular automata (CA) model was imported into Deform-3D commercial finite element simulation software and the microstructure evolution was simulated in the process of thermal compression and accumulative rolling-bonding.

**Key words:** TA15 titanium alloy; accumulative roll bonding; numerical simulation; cellular automata

Titanium alloys possess high specific strength, thermal stability and corrosion resistance, and have been increasingly used as key structural parts in aerospace, automotive, and biomedical applications<sup>[1,2]</sup>. With the development of modern manufacturing industry, the sheet production has accounted for more than 50% of the titanium processing market<sup>[3]</sup>. Lightweight, high energy, and low cost have gradually become the main optimization objectives of primary load-carrying sheet structures. Such structures are extremely demanded in terms of mass, integrity and cost, which lead to a narrow processing window of the sheets. In addition, it is difficult to obtain the ultra-fine crystal sheets because of poor plasticity at room temperature and low equivalent strain under the traditional rolling process conditions. Therefore, the superior superplastic forming ability of the prepared sheets is difficult to obtain under such conditions. Therefore, the accumulative roll bonding (ARB) process was explored to solve these problems by preparing the ultra-fine grain (UFG) sheets of titanium alloy<sup>[4]</sup>.

In the past 30 years, the severe plastic deformation (SPD) technology has been investigated over a wide range. The typical SPD technologies mainly include high pressure torsion (HPT), multi-directional compression/forging (MF), equal

channel angular pressing (ECAP), torsion extrusion (TS), continuous shear deformation (CP) and accumulative roll bonding (ARB)<sup>[5]</sup>. The ARB technology and CP technology are generally suitable for preparing sheet with UFG structure among them. The ARB process was first proposed by Saito<sup>[6]</sup> in 1999, and the process route was achieved by repeated rolling and welding. The strengthening mechanism is that the matching of high strength and high toughness is implemented by refining the grain size to submicron or even to nanometer level under a certain process window. Compared with other SPD technologies, the ARB technology provides more advantages of simple process, low requirement of equipment and obvious grain refinement, which is a promising technology for UFG sheet production.

In recent years, a lot of researches about the preparation process of ARB technology have been studied. Based on the theoretical derivation of equivalent strain, Xiang et al<sup>[7]</sup> successfully obtained the UFG sheets of pure aluminum, aluminum alloy and ultra-low carbon steel by changing the interface number, layer distance, cumulative strain and other variables in the ARB forming process. Xing<sup>[8]</sup> and Kwan et al<sup>[9]</sup> predicted the failure mode of ARB forming process by

Received date: March 03, 2021

Foundation item: National Natural Science Foundation of China (51471136)

Corresponding author: Zhao Yongqing, Ph. D., Northwest Institute for Nonferrous Metal Research, Xi'an 710016, P. R. China, Tel: 0086-29-86266577, E-mail: trec@cn-nin.com

Copyright © 2021, Northwest Institute for Nonferrous Metal Research. Published by Science Press. All rights reserved.

analyzing the interface morphology under different thermal parameters. Tsuji et al.<sup>[10]</sup> found that the number of stacked layers is closely related to the grain refinement through the ARB experiments with 1 mm thick sheets. After studying ARB forming process for different materials, Lee et al.<sup>[11]</sup> discovered that the microstructure of aluminum alloy and steel sheet is strip-shaped, and the grains are extended obviously in longitudinal direction. It can be seen that the evolution of the microstructure, the evolution mechanism of the bonding interface, the traceability of crack propagation have been studied to a large degree in the current ARB process research of the titanium alloy sheet, but there are few reports on the prediction of thermal parameters and microstructure.

Apart from experimental analyses, a powerful research tool for microstructure modeling, finite element model, has been developed, but it has less application in ARB simulation<sup>[12]</sup>. Wang et al.<sup>[13]</sup> applied the crystal plasticity finite element method to the ARB-induced polycrystalline microstructure, and obtained polycrystalline microstructure similar to the experimental one. Wang et al.<sup>[14]</sup> established finite element model of multi-cycle ARB using a mapping solution technique, and successfully simulated the texture and hardness in the ARB process for five cycles.

Hence, the ARB finite element model of TA15 alloy sheet was established in terms of the constitutive relation of thermo-mechanical coupling and accurate boundary conditions. Moreover, the distribution of thermal parameters under different process conditions was analyzed by numerical simulation, and the microstructure was predicted and verified by the cellular automata (CA)<sup>[15]</sup> model, so as to obtain the evolution rule of thermal parameters and the prediction model of microstructure of TA15 alloy during ARB forming process. This study provide a powerful route to investigate the microstructure evolution and process optimization in accumulative roll-bonding of TA15 sheets.

## 1 Method

### 1.1 Coupled thermo-mechanical FE modeling

The material used was TA15 alloy with a composition (wt%) of 6.46Al-2.12Zr-1.12Mo-1.21V. It was received as the twice hot-rolled sheet with the size of 3000 mm×3000 mm×14.5 mm. The specimen was first heated to 1010 °C for 2 h, then cooled to 925 °C for 2 h, and finally water cooled to room temperature. The water cooling after heating was to ensure that the obtained microstructure at high temperatures is retained. The phase transformation temperature was measured at 995 °C by metallographic observation method in laser confocal high-temperature scanning microscope (Lasertech Inc., Yonekura, Japan). Fig. 1 shows the Widmanstatten structure after heat treatment, and the thickness of lamellae is determined to be 1.1 μm measured by Image-Pro Plus image analysis software.

Cylindrical specimens with  $\Phi 8$  mm×12 mm were cut from the as-received and heat treated material by wire-electrode cutting. The isothermal compression was carried out on a

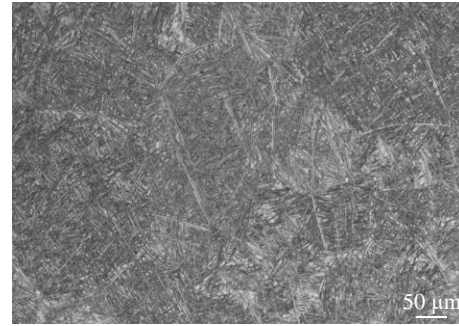


Fig.1 Microstructure of TA15 sheet after heat treatment

Gleeble-3800 machine (Dynamic Systems Inc., North Carolina, America) at 800, 850, 900, 930, and 960 °C, and strain rates of 0.001, 0.1, 1, and 10 s<sup>-1</sup>. The experiment maintained the heating rate as 10 °C/s and then the sample was soaked for 3 min. The flow stress curves at 850 and 930 °C produced by this treatment are shown in Fig. 2. The constitutive model of thermal deformation for TA15 sheet was determined by a dependence-based integrated constitutive modeling methodology<sup>[16]</sup>. The used equipment of ARB of TA15 sheets was 6-high CVC plus reversing cold rolling machine (SMS Siemag Technology (Beijing) Co., Ltd, Beijing, China).

### 1.2 Thermo-mechanical modeling of ARB

The thermo-elasto-plastic coupling equations for ARB are established based on the virtual work principle and large deformation theory, with the following form:

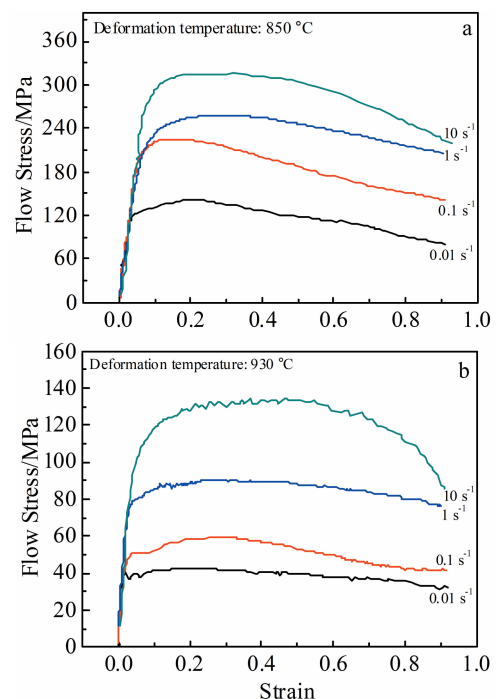


Fig.2 True stress-strain curves of TA15 sheet at 850 °C (a) and 930 °C (b)

$$\left( [K_{ep}] + [K_G] \right) \{ \dot{d} \} = \int_V [B_e]^T \{ \dot{\epsilon}^T \} dV - \int_V [B_e]^T \{ \dot{R}_{\epsilon T} \} dV + \{ \dot{F}_0 \} \quad (1)$$

where  $K_{ep}$  is elastoplastic stiffness matrix,  $K_G$  is geometric stiffness matrix,  $\dot{d}$  is node velocity,  $\dot{R}_{\epsilon T}$  is change rate relative to temperature and equivalent plastic strain rate,  $B_e$  is strain matrix, and  $\dot{F}_0$  is rate of external load change.

Coulomb friction assumed that the pressure of the contact surface is directly proportional to the friction, expressed by

$$F = \mu |\sigma_n| \left( \left| \mu |\sigma_n| < \frac{Y}{\sqrt{3}} \right. \right) \quad (2)$$

where  $\mu$  is the coulomb friction coefficient,  $Y$  is the shear yield limit of material, and  $\sigma_n$  is the normal stress on the friction surface.

Arctangent friction model of relative sliding velocity can be expressed by:

$$F = -mK \left\{ \frac{2}{\pi} \tan^{-1} \left( \frac{|v_s|}{av_0} \right) \right\} \frac{v_s}{|v_s|} \quad (3)$$

where  $m$  is the arctangent friction factor,  $K$  is the shear yield strength of material,  $v_s$  is the relative speed,  $v_0$  is the absolute

value of rolling speed and  $a$  is tuning parameter, generally  $10^{-5}$ .

The flow stress of the treated sheet was imported into the material library of Deform-3D software. In traditional rolling process, the friction is generally defined as shear friction when the sheet contacts with roller and push sheet<sup>[17]</sup>. However, the friction factor is defined by the combination of shear friction and coulomb friction due to the relative friction between different sheets in the cumulative rolling process (as shown in Table 1). Combined with the boundary conditions and simulation parameters acquired previously, the cumulative rolling finite element model of TA15 sheet was established (as shown in Fig. 3). The left, right and surface boundaries of TA15 sheet are free boundary, but have heat exchange with the surrounding environment. The surrounding environment and the boundary condition in the center are to limit the displacement in the  $y$  direction. The thickness of the TA15 sheet is 14.5 mm, and the length is 1200 mm. The mesh uses quadrilateral structural elements in Deform-3D. The minimum and maximum sizes of element are 0.9 and 6.3  $\mu\text{m}$ , respectively, and the total number of element is 54 342.

**Table 1** Boundary conditions and simulation parameters<sup>[17-19]</sup>

	Setting	Value
Boundary condition	Convection coefficient/ $W \cdot (m^2 \cdot K)^{-1}$	20
	Thermal conductivity of roller/ $W \cdot (m \cdot K)^{-1}$	51.9
	Thermal radiation from environment	0.25
	Coulomb friction	0.3
	Arctangent friction	0.5
Simulation parameter	Roller radius, $R/\text{mm}$	415
	Rolling speed, $v_0/\text{m} \cdot \text{s}^{-1}$	1.5, 2.0, 2.5
	Rolling temperature/ $^{\circ}\text{C}$	800, 850, 900
	Thickness reduction/%	10, 20, 30, 40, 50

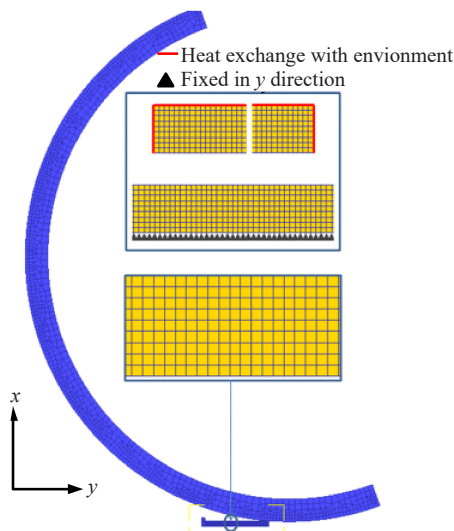


Fig.3 FEM model and boundary conditions

The schematic diagram of the deformation area during accumulative rolling process is summarized in Fig.4. Therefore, it is difficult to investigate the deformation of the same section based on time because of different rolling direction (RD) positions. In general, 1/2 of the sum of biting angle and neutral angle can be selected as a reference. Table 2 lists the process parameters of ARB under different thickness reduction.

### 1.3 Cellular automata modelling of microstructure in ARB process

Cellular automata (CA) model is a grid dynamic model with discrete space-time situation and local spatial interaction, which particularly embody practical causality. In recent years, it has become an important method to predict the evolution of structure through the flexible adaptation to space-time scale.

The dynamic globularization can be divided into two stages: fracture nucleation and growth of lamellar. In order to simplify the simulation process, the dynamic globularization model adopts the following assumptions: the dislocation

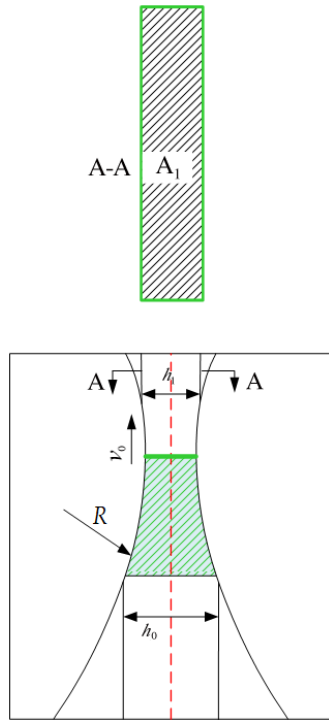


Fig.4 Schematic diagram of ARB deformation zone

Table 2 Process parameters of ARB

Thickness reduction/%	Biting angle/(°)	Neutral angle/(°)	Sectional area/m <sup>2</sup>
10	3.72	1.78	2.73
20	5.21	2.40	3.81
30	6.43	2.90	4.65
40	7.34	3.31	5.28
50	8.22	3.61	5.90

density in matrix can conform to Kocks-Mecking equation<sup>[20]</sup> in the recovery stage because of its identity. The fracture nucleation of lamellar occurs when the dislocation density reaches the criticality. Also, the initial dislocation matrix of the material with lamellar fracture nucleation is set as  $2 \times 10^9 \text{ m}^{-2}$ , and the dislocations in the grains are uniformly distributed without gradient. On the one hand, the decomposition of the lamellar adopts the combination of grain boundary sliding, bending separation and straight separation. On the other hand, the lamellar existing in grain boundary is dominated by the grain boundary sliding and the intragranular lamellae are influenced by both bending separation and straight separation. Furthermore, the program diagram of CA model can be established according to the above assumptions (Fig.5).

The polycrystal plasticity FE model is established based on Hill's quadratic anisotropy yield function<sup>[20]</sup>, which includes the microstructural texture information on texture and crystal type. The orientation distribution function is calculated at the material point in the meshed stress space.

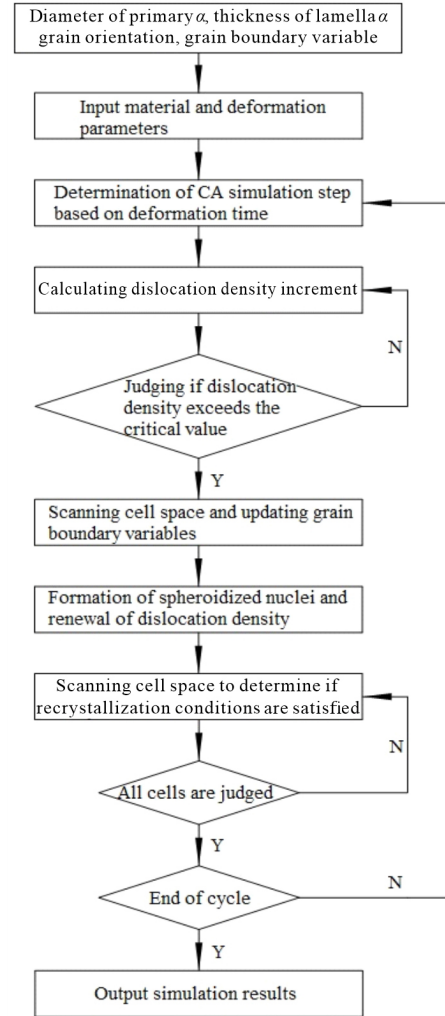


Fig.5 CA model block diagram

$$\phi = F(\sigma_{yy} - \sigma_{zz})^2 + G(\sigma_{zz} - \sigma_{xx})^2 + H(\sigma_{xx} - \sigma_{yy})^2 + 2L\sigma_{yz}^2 + 2M\sigma_{zx}^2 + 2N\sigma_{xy}^2 \quad (4)$$

where  $F, G, H, L, M$  and  $N$  are the anisotropic constants.

The dynamic recrystallization adopts the nucleation model proposed by Ding and Guo<sup>[21]</sup>.

$$\dot{n}(\dot{\epsilon}, T) = C\dot{\epsilon}^m \exp\left(-\frac{Q_{act}}{RT}\right) \quad (5)$$

where  $C$  and  $m$  are material constants,  $Q_{act}$  is activation energy,  $\dot{n}$  is nucleation rate,  $\dot{\epsilon}$  is strain rate,  $T$  is temperature, and  $R$  is Stefan-Boltzmann constant.

In order to simplify the CA microstructure model constructed, this work adopts the following assumptions: (1) the rotation of crystal grains is ignored; (2) there is no texture in the deformed microstructure, and the influence of texture on dynamic recrystallization in the actual deformed structure is ignored; (3) only the dislocations, crystal grains, grain boundaries and second phase particles existing in the crystal are considered, and the defects such as vacancies, interstitial atoms, stacking faults, twins are ignored; (4) only the dislocation density changes caused by dynamic recovery are considered, and its impact on microstructure changes is

ignored.

The region was divided into a quadrilateral cell space of  $200\ \mu\text{m} \times 200\ \mu\text{m}$  and the corresponding size of each mesh was determined as  $1.0\ \mu\text{m} \times 1.0\ \mu\text{m}$ . The structure of initial grain was obtained by supersaturated nucleation and growth through CA method. The CA model takes the field variables calculated from the thermo-mechanical coupling FE model as input variables. That is, the FEM calculated the field variables such as strain, strain rate, and temperature. These field variables are used for the input of CA model. The big model in FEM is used to obtain the averaged results for fields, thus improving the calculation accuracy of small CA model.

## 2 Process Simulation Results and Discussion

The distribution of thermal parameters from the normal direction (ND) to RD can directly reflect the deformation process of the accumulative rolling process. The influence rules of the process parameters on stress, strain, strain rate and temperature field were established using the accurate finite element model to simulate the cumulative rolling process of TA15, and thus the measures to improve the homogeneity of microstructure can be obtained in the cumulative rolling process of TA15.

### 2.1 Effect of deformation on ARB process

The change of the equivalent stress of  $A_1$  section in ND direction is illustrated in Fig.6. It can be seen that the surface stress is lower than the central stress, and the central stress increases with the increase of deformation. However, as for the stress distribution of traditional rolling process, the surface stress is generally higher than the center stress. The heat generated by surface friction is difficult to be transmitted to the interior through the way of heat conduction which is due to poor thermal conductivity of  $6.7\ \text{W}/(\text{m}\cdot\text{K})$  for titanium alloy. Moreover, the high strain rate generated by the accumulated rolling process makes the surface generate adiabatic temperature rise, which will further lead to the rapid rise of temperature and the reduction of equivalent stress. With the increase of deformation, the contact length between rolling piece and roll keeps rising, and the effect of rising temperature is also expanded. For the central stress, the higher deformation corresponds to the larger deformation area.

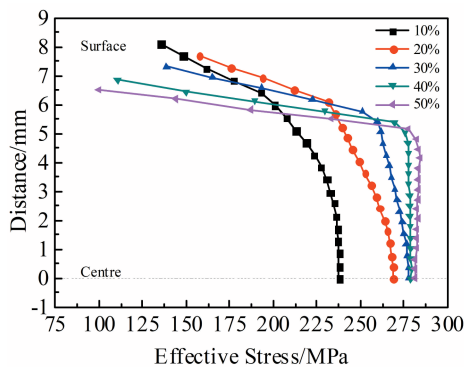


Fig.6 Equivalent stress under different thickness reduction

Therefore, the central stress reaches a higher value because of the larger rolling pressure and average unit pressure.

Fig. 7 shows the change of the equivalent stress of the central node with the rolling time at different deformation conditions. In Fig.7, the signs of  $t_1, t_2, t_3, t_4$  and  $t_5$  correspond to the rolling time of the cross section under five kinds of deformation. From Fig. 7, the geometric parameters (length/width) of the rolling deformation zone and the rolling time of the section in the rolling deformation zone all increase with the increase of deformation. During the period of stable rolling in the deformation zone, the larger the deformation, the higher the equivalent stress. In addition, the equivalent stress becomes higher when it is closer to the narrowest part of the wedge-shaped deformation zone with the rolling processing. The equivalent stress fluctuates significantly in two sections of entering and leaving the deformation zone, which is determined by two unstable stages of biting in and throwing out.

Fig. 8 represents the variation of equivalent plastic strain along the direction of ND under different thickness reduction. The distribution of the total equivalent effect and the variation of strain in the direction of thickness all present a rising trend as the deformation increases. The growth rate curves of strain show the growth laws that the deformation is characterized by an uneven increase. Because the simulation result is obtained under the single pass deformation, the conclusion can be derived that the strain gradient in thickness direction is affected by the deformation passes. Therefore, excessive

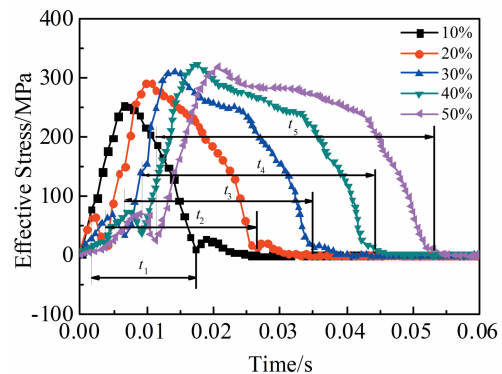


Fig.7 Variation of equivalent stress along the center line

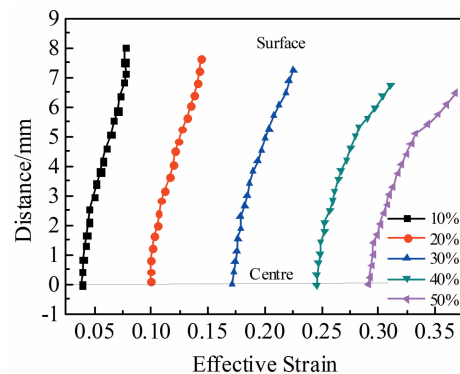


Fig.8 Equivalent strain along the ND direction

deformation of the rolling pass should be avoided in the design of cumulative rolling to reduce the strain gradient.

Fig.9 shows the distribution of the equivalent plastic strain in centre and surface changing with time under the conditions of different thickness reduction. It can be seen that the equivalent plastic strain of both surface layer and central layer increases with the rolling time. With the increase of thickness reduction, the difference of the strain between centre and surface enlarges step by step, and the growth of centre is larger than that of surface, which leads to the uneven deformation in the thickness direction.

Fig.10 gives the distribution of shear strain of the RD-ND surface along ND direction in the section. It is obvious that the shear strain displays the similar behavior with the increase of deformation.

It should also be noted that a significant difference of the direction of shear strain occurs in the two sides of the intersection (at a thickness of 6 mm). This particular distribution is closely related to the characteristics of cumulative rolling. According to previous studies, friction force is the driving force of cumulative rolling and it belongs to the surface shear stress. The effect of friction force is attributed to the excellent ductility of rolled piece surface, but there is a spread gradient between single sheet and multi-layer sheet in

the thickness direction. Therefore, the transformation of shear strain exists in the intersection. As clearly observed from the influence of deformation on thermal parameters, small deformation with the single pass can effectively improve the non-uniformity of distribution.

**2.2 Effect of rolling speed on ARB process**

The effect of rolling speed on equivalent stress along ND direction is presented in Fig.11. It shows that the equivalent stress increases along with the increase of rolling speed and the growth of centre is significantly higher than that of surface.

According to the distribution of temperature field shown in Fig.12, high temperature makes the metal flow and softening can be observed. Furthermore, the strain rate from surface to centre presents the evolution law of decreasing first and then increasing, which is influenced by the temperature change (Fig.13). In terms of the thermo-mechanical coupling and constitutive law, TA15 alloy has a high sensitivity to strain rate and deformation temperature. While the stress in the surface produced with high strain rate is offset by the high temperature, which directly results in the stress to stop growing or even to decrease. According to the influence of rolling speed on thermal parameters, temperature distribution from the centre to the surface can be improved by lowering rolling speed.

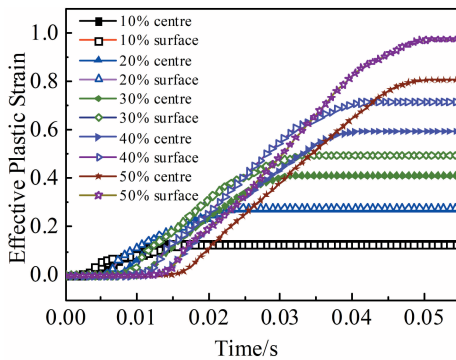


Fig.9 Distribution of equivalent plastic strain in centre and surface with time

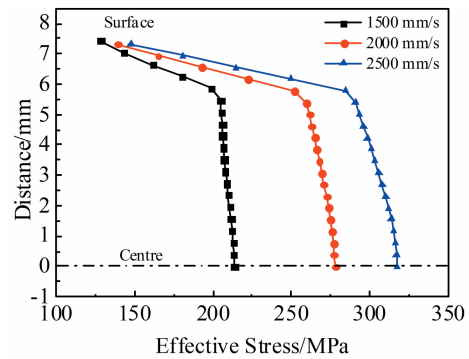


Fig.11 Equivalent stress along ND direction under different rolling speeds

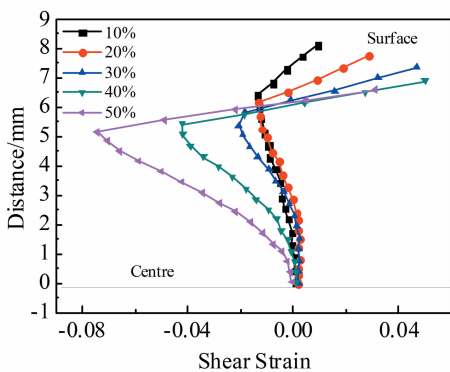


Fig.10 In-plane shear strain along ND direction under different thickness reduction

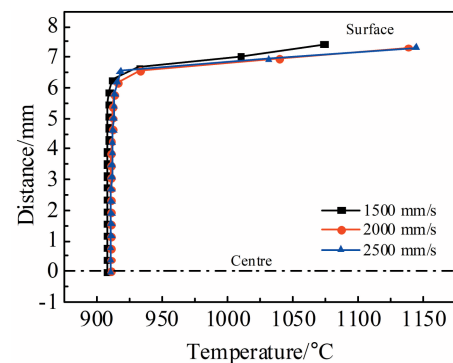


Fig.12 Temperature field along ND direction under different rolling speeds

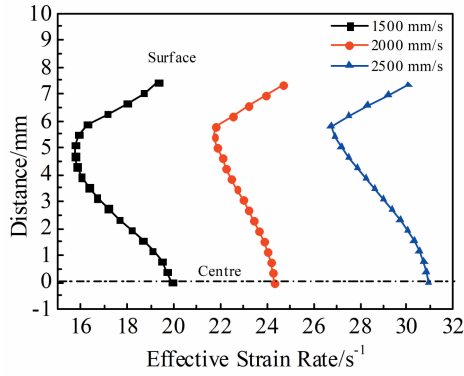


Fig. 13 ND strain rate distribution under different rolling speeds

### 2.3 Effect of rolling temperature on ARB process

Fig. 14 represents the distribution of equivalent stress and equivalent strain along the ND direction at different rolling temperatures. The equivalent stress of the section decreases as the rolling temperature increases for the same deformation area. However, the distribution of strain exhibits an opposite trend, i.e. it is lower in center while higher in surface. In addition, the strain range increases simultaneously with the increase of rolling temperature and deformation of centre and surface.

It can be seen from Fig. 15 that the temperature rise of the sheet shows a trend of being lower in center and being higher in surface, which also indicates that the temperature rise of the

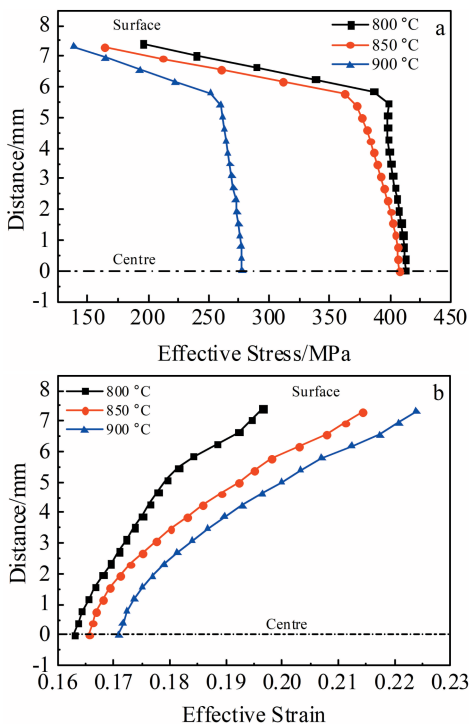


Fig. 14 Equivalent stress (a) and equivalent strain (b) distribution along ND direction

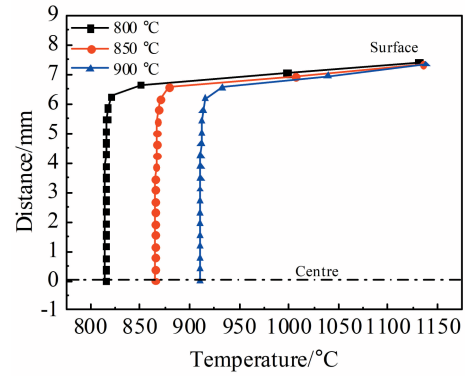


Fig. 15 Temperature distribution under different rolling temperature conditions along ND direction

surface is mainly derived from the high strain rate caused by high-speed cumulative rolling, thus leading to the “skin effect” in the superficial area. From the influence law of rolling temperature on the thermal parameters, the medium rolling temperature can effectively improve the strain and temperature range of the accumulative roll-bonding sheets, so as to obtain the optimal structure property.

### 3 CA Microstructure Simulation Results and Discussion on ARB Process

According to the comparison from the above results, the grain size of 9.2, 13.6, and 18.9  $\mu\text{m}$  can be obtained before the hot deformation at 800, 850, and 900  $^{\circ}\text{C}$ , respectively. Based on the assumption and simplification from the dynamic globularization above, the change of microstructure of TA15 alloy under different conditions (temperature of 800, 850, and 900  $^{\circ}\text{C}$ ; strain rate of 0.01, 0.1, 1, and 10  $\text{s}^{-1}$ ) was simulated by CA model during the dynamic recrystallization.

From the comparison between the simulation results and experiment results in Fig. 16, the results of CA simulation have a high advantage in accuracy in terms of grain morphology and volume fraction of recrystallization. On condition that the macro data of rolling stress, strain and temperature field can be extracted, the simulation analysis of microstructure of rolled sheet can also be achieved. The microstructure under optical microscope (OM) is similar to that under CA simulation, in which the proportion of primary phase is less, and the overall deformation direction of matrix is perpendicular to compression reverse. Fig. 16c shows that equiaxed grains with an average size of about 0.86  $\mu\text{m}$  can be observed in the area with large deformation. This prediction model is reliable when we combine the microstructure of characteristic points in Fig. 16b with the analysis of Fig. 16a.

Finally, it can be seen from Fig. 17 that the continuous process of dynamic recrystallization is maintained on the grain boundary with the increase of strain, and the recrystallization grain grows gradually. Hence, the average grain size and volume fraction of the recrystallized grain increase steadily.

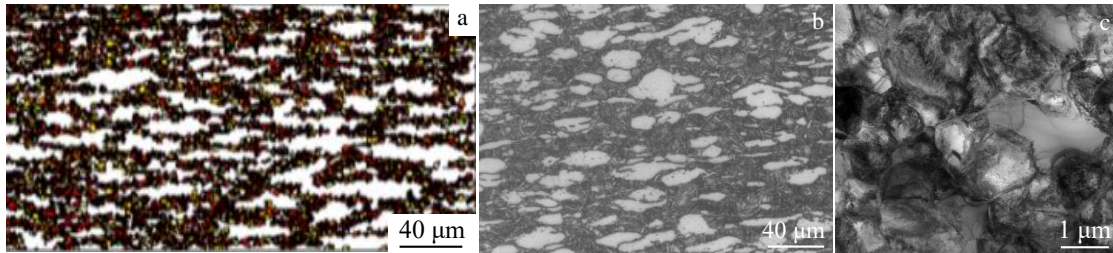


Fig.16 Comparison of forming state microstructure under 800 °C/1 s<sup>-1</sup>: (a) CA simulation, (b) OM microstructure, and (c) TEM microstructure

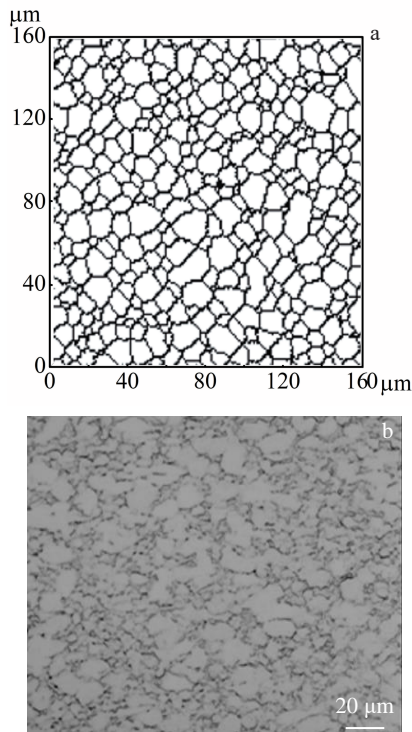


Fig.17 Microstructure comparison under 930 °C/1 s<sup>-1</sup>: (a) CA simulation and (b) metallographic microstructure

#### 4 Conclusions

1) The thermal parameters and the microstructure evolution in ARB process of TA15 alloy are predicted using finite element simulation software of Deform-3D, as implemented by the combination of thermo-mechanical FEM and cellular automata model.

2) A small thickness reduction in single pass ARB can effectively improve the nonuniformity of shear strain distribution, and the shear strain displays the similar behavior with the increase of deformation. The temperature distribution from the centre to the surface can be improved by lowering rolling speed.

3) The microstructure and properties of TA15 alloys can be effectively improved by reducing the thickness reduction (<30%), lowering rolling speed (<2000 mm/s), and maintaining a certain temperature (800 °C). The microstructure obtained by CA simulation is similar to that experimentally

observed.

#### Reference

- 1 Yi J, Wang X B, Jiao L et al. *Thin-walled Structures*[J], 2019, 144: 106 329
- 2 Xiang J F, Yi J. *CIRP Journal of Manufacturing Science and Technology*[J], 2021, 32: 356
- 3 Fan X G, Yang H, Gao P F. *Journal of Materials Science*[J], 2011, 46: 6018
- 4 Zhou Xiaolong, Tao Qiying, Zhou Yunhong. *Rare Metal Materials and Engineering*[J], 2017, 46: 942
- 5 Xiang J, Pang S, Xie L J. *The International Journal of Advanced Manufacturing Technology*[J], 2018, 97: 1673
- 6 Saito Y, Utsunomiya H, Tsuji N. *Acta Materialia*[J], 1999, 47: 579
- 7 Xiang J, Pang S, Xie L J. *The International Journal of Advanced Manufacturing Technology*[J], 2018, 98: 1237
- 8 Xing Z P, Kang S B, Kim H W. *Metallurgical and Materials Transactions A*[J], 2002, 33: 1521
- 9 Kwan C, Wang Z, Kang S. *Materials Science and Engineering A* [J], 2008, 480: 148
- 10 Tsuji N, Saito Y, Lee S H. *Advanced Engineering Materials*[J], 2003, 5: 338
- 11 Lee S H, Saito Y, Tsuji N. *Scripta Materialia*[J], 2002, 46: 281
- 12 Xiang J F, Xie L J, Gao F. *Chinese Journal of Aeronautics*[J], 2020, 34(8): 218
- 13 Wang H, Lu C, Tieu K. *Crystals*[J], 2019, 9: 119
- 14 Wang H, Su L, Yu H et al. *Materials Science and Engineering A* [J], 2018, 726: 93
- 15 Khatami R, Fattah-Alhosseini A, Mazaheri Y. *The International Journal of Advanced Manufacturing Technology*[J], 2017, 93: 681
- 16 Xiang J, Xie L, Gao F et al. *Ceramics International*[J], 2018, 44: 5341
- 17 Yi J, Xiang J, Yi F et al. *The International Journal of Advanced Manufacturing Technology*[J], 2018, 97: 1673
- 18 Xiang J, Xie L, Gao F et al. *Ceramics International*[J], 2019, 44: 117 65
- 19 Xiang J, Pang S Q, Xie L J. *Materials*[J], 2018, 11: 252
- 20 Mecking H, Kocks U F. *Acta Metallurgica*[J], 1981, 29: 1865
- 21 Ding R, Guo Z X. *Acta Materialia*[J], 2001, 49: 3163

## 基于元胞自动机的TA15板材累积叠轧微观组织预测

韩 栋<sup>1</sup>, 赵永庆<sup>1,2</sup>, 曾卫东<sup>1</sup>, 李 磊<sup>2</sup>, 张永强<sup>2</sup>

(1. 西北工业大学 材料学院, 陕西 西安 710072)

(2. 西北有色金属研究院, 陕西 西安 710016)

**摘 要:** 为研究累积叠轧过程中TA15钛合金微观组织的演变规律, 首先利用DEFORM有限元软件模拟了不同累积叠轧工艺对板材成形热参数的影响, 在此基础上通过元胞自动机模拟了TA15钛合金累积叠轧后组织的动态球化过程。结果表明, 在累积叠轧过程中, 通过减少单道次变形、降低轧制速度并保持一定的温度, 可有效地改善TA15钛合金的微观组织和性能。将元胞自动机动态球化模型导入Deform-3D软件, 成功地模拟了在热压缩和累积叠轧过程中微观组织的演变。

**关键词:** TA15钛合金; 累积叠轧; 数值模拟; 元胞自动机

**作者简介:** 韩 栋, 男, 1981年生, 博士生, 高级工程师, 西北工业大学材料学院, 陕西 西安 710072, 电话: 029-88494298, E-mail: hand227@163.com